Geophys. J. Int. (2007) **169,** 926–940 doi: 10.1111/j.1365-246X.2007.03334.x

Deep resistivity structure of the Trans-European Suture Zone in Central Poland

P. Yu. Pushkarev,[1] T. Ernst,[2] J. Jankowski,[2] W. Jozwiak,[2] M. Lewandowski,[2,3] K. Nowozynski[2] and V. Yu. Semenov[2]

[1] *Geological faculty of Moscow State University, Leninskiye Gory* 1, 199992 *Moscow, Russia. E-mail: pavel˙pushkarev@mtu-net.ru*
[2] *Institute of Geophysics, Polish Academy of Sciences, Ks. Janusza* 64, 01-452 *Warszawa, Poland*
[3] *Institute of Geological Sciences, Polish Academy of Sciences, Twarda* 51/55, 00-818 *Warszawa, Poland*

Accepted 2006 December 13. Received 2006 December 12; in original form 2006 January 2

SUMMARY

The deep resistivity structure was estimated along a 400-km profile in central Poland crossing the Malopolska Massif (MM), the Lysogory Unit (LU), the Trans-European Suture Zone (TESZ) and ending at the East European Craton (EEC). Magnetotelluric transfer functions, corresponding to 20 sites, were supplemented by magnetovariational responses obtained at the geomagnetic observatories situated at the same tectonic units. Such a combination made it possible to extend the initial period range, which is from fractions of a second to several hours, up to months in order to reliably cover crustal and upper-mantle depths. The geoelectrical structures, revealed using 2-D inversions, do not contradict the known features of the lithosphere structure determined using seismic and gravity data along the profile.

The subsurface conductance, varying from approximately 10 Siemens at the inner part of the EEC to about 600 Siemens in the TESZ, is produced by sediments, the deep part of which contains conductive, highly mineralized water. The existence of two crustal conductive faults at the southwest and northeast of the TESZ were established mainly by the use of induction arrows. It was also revealed that rather high mantle conductivity beneath the MM, LU and TESZ at depths of about 150–200 km contrasts with the resistive upper mantle of the EEC. This can be interpreted as the decrease of asthenosphere conductance and/or as its submersion beneath the EEC. Generally, the results confirm the idea that the TESZ forms not only specific seismic boundaries but also causes peculiar conductivity anomalies in the crust and upper mantle.

Key words: asthenosphere, continental crust, electrical conductivity, electromagnetic induction, magnetotellurics, Trans-European Suture Zone.

INTRODUCTION

The Trans-European Suture Zone (TESZ) is a major lithospheric boundary, stretching from the Black Sea in the southeast to the British Isles in the northwest (Dadlez *et al.* 1994; Pharaoh 1999). In a general sense, it can be correlated with the Appalachian orogen in North America (Keller & Hatcher 1999). In Poland, the TESZ separates the Precambrian East-European Craton (EEC) from younger, Phanerozoic tectonic structures (Fig. 1). Seismic results obtained from the POLONAISE'97 project enabled insight into the deep structure of the TESZ in Poland (Guterch *et al.* 1999). It was established that this zone can be traced at least down to the Moho (30–50 km). Crystalline basement depression and significant Moho depth gradient were revealed here, and evidence for the southwestern extension of the lower crust of the EEC beneath the younger structures was also found (Grad *et al.* 2003). The international seismic project CELEBRATION 2000 was planned to extend the investigation depth to 50–100 km (Guterch *et al.* 2001).

Seismic tomography results (Zielhuis & Nolet 1994) show that low *S*-wave velocities are a characteristic feature of the upper mantle beneath Phanerozoic Europe, while higher *S*-wave velocities occur beneath the EEC. The abrupt change of these velocities coincides with the boundary of the TESZ and EEC. This boundary is also clearly visible on gravity and magnetic field maps (Krolikowski *et al.* 1999; Wybraniec 1999). The analysis of heat flow data on Polish territory shows that it gradually increases when we move from the EEC to the younger structures in the southwest (Plewa *et al.* 1995; Gordienko & Zavgorodnaya 1996; Majorowicz 2004).

Studies of magnetic field variations in Poland were initiated by J. Jankowski in 1960. They led to the discovery of two conductive anomalies. The first one is associated with the TESZ and is located in the upper crust of northwestern Poland (Jankowski 1967). It was traced using induction arrows and its nature was explained by the

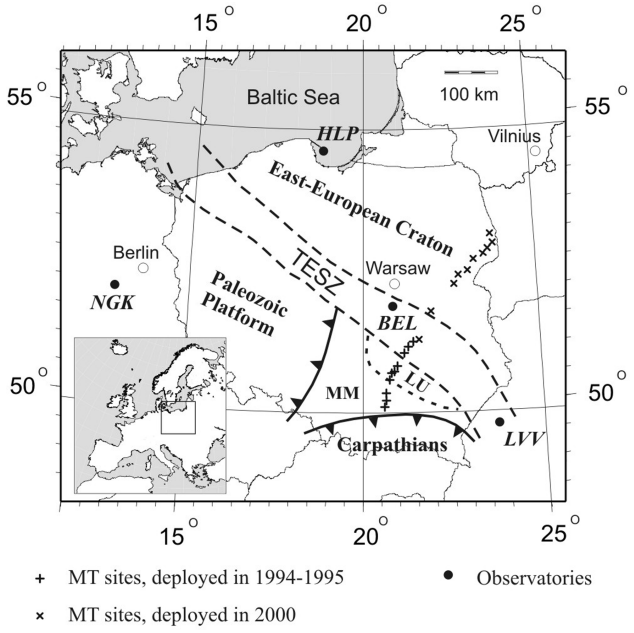

Figure 1. Location of MT sites and geomagnetic observatories. Tectonic structures include: MM, Malopolska Massif; LU, Lysogory Unit.

sediments of the Polish Basin (Jankowski 1965). The second one is the Carpathian conductive anomaly, and its induction studies were performed in Poland and in other countries (Rokityanskiy *et al.* 1975; Jankowski *et al.* 1985).

Numerous magnetotelluric (MT) soundings were performed by the Geophysical Research Enterprise of Warsaw. However, these studies focused on the depth of the crystalline basement. Investigation of deep structures started from an analysis of data obtained at the Polish geomagnetic observatory of Belsk (Schmucker & Jankowski 1971). Later, MT soundings were carried out along several regional profiles, including the Tatra Mountains (Ernst *et al.* 1997), Holy Cross Mountains (Semenov *et al.* 1998), TESZ in southeastern Poland (Ernst *et al.* 2002) and EEC (Semenov *et al.* 2002; Jankowski *et al.* 2004). The results of soundings performed along seismic profile P4 of the POLONAISE'97 project have just been analysed (Semenov & Jozwiak 2005).

Recently, electromagnetic measurements were performed within two international projects to study the resistivity structure of the TESZ. In the Central Europe Mantle geoElectrical Structure (CEMES) project, deep electromagnetic soundings were performed at 14 geomagnetic observatories situated in the TESZ and its vicinity in nine countries (Semenov *et al.* 2003). Detailed MT observations were performed along several profiles in northwestern Poland within the EMTESZ-Pomerania project (Varentsov *et al.* 2004).

In this paper, we discuss the construction of a resistivity model for the TESZ and its surroundings in central Poland. To this end we consider a 400-km-long profile that stretches from the Carpathians in the southwest to the EEC in the northeast (Fig. 1). From southwest to northeast, the profile runs from the Malopolska Massif (MM) through the Lysogory Unit (LU) and several subsurface units north of the Lublin trough, as to Krakow-Ratno horst and Podlaskie trough, ending with the thin sediments in the Mazursko-Belarusian anticline. It roughly coincides with seismic profile C01 deployed during the CELEBRATION project. The results of these seismic studies, with detailed geological and geophysical information about the area, are presented in (Sroda *et al.* 2006). The interpretation of gravity and magnetic data had been performed previously along approximately the same profile and increased magnetic and density properties were revealed in the southwest of the TESZ (Grabowska & Bojdys 2001).

The southwestern 10 sites of the MT profile were deployed in 1994–1995, and the northeastern 10 sites were deployed in 2000. These two data sets were previously interpreted separately. The interpretation of the first data set provided only a rough idea of the deep resistivity structure of the TESZ, as the appropriate profile reaches this zone but does not cross it, being a study of the Holy Cross Mountains region (Semenov *et al.* 1998). The second data set had the same problem, as it was obtained to study the EEC; besides, its analysis focused only on either shallow or deep structures, and high-frequency data were not used (Semenov *et al.* 2002; Jankowski *et al.* 2004). Now, we present the results of joint interpretation of all these data targeted at constructing a resistivity model of the TESZ. To obtain more reliable results at upper-mantle depths, we also consider the results of magnetovariational soundings performed at the nearest geomagnetic observatories.

Equipment designed at the Belsk observatory was used to obtain data (Marianiuk 1977, 2000). Telluric lines approximately 100 m long were used for electric field measurements. The magnetic field was measured using three-component quartz magnetometers at low frequencies (sampling interval 1 s). The duration of each deep sounding was about 3 weeks. At the 10 northeastern sites, high-frequency horizontal field components were also recorded using induction coils (sampling interval 0.005 s). In this paper, we consider transfer functions estimated using the frequency-domain processing technique (Semenov & Kaikkonen 1986). Magnetic field responses had previously been compared with results obtained using the time domain technique (Wieladek & Ernst 1977) and the agreement was good.

DATA ANALYSIS

The general purpose of the data analysis is to construct a data set to be used in further interpretation. As it is not expedient to perform 3-D inversion of data obtained along one profile, and to include local near-surface inhomogeneities into the interpretational model, we first needed to estimate the applicability of 1-D and 2-D approximations and to evaluate near-surface distortions.

We will operate with impedance $[Z]$ and tipper $[W]$ matrices with their complex components characterizing resistivity distribution in the Earth and satisfying the equations for complex amplitudes of electromagnetic field components:

$$E_X = Z_{XX} \cdot H_X + Z_{XY} \cdot H_Y,$$
$$E_Y = Z_{YX} \cdot H_X + Z_{YY} \cdot H_Y,$$
$$H_Z = W_{ZX} \cdot H_X + W_{ZY} \cdot H_Y,$$

where E_X and E_Y are horizontal electric field components, H_X and H_Y are horizontal and H_Z is the vertical magnetic field component. Throughout this paper we use a coordinate system in which the X-axis is directed north and Y-axis is directed east. A factor $\exp(-i\omega t)$ is assumed here for time-varying functions.

For the convenience of further analysis and inversion, MT transfer functions were recalculated to a uniform and common for all sites grid of periods using a robust smoothing method. As an example, the phases and magnitudes of impedance components Z_{XY} and Z_{YX}, corresponding to sites 01 (situated at MM) and 14 (situated at EEC), are presented in Fig. 2. In general, the quality of the impedance data is not high because the electric field is disturbed by industrial

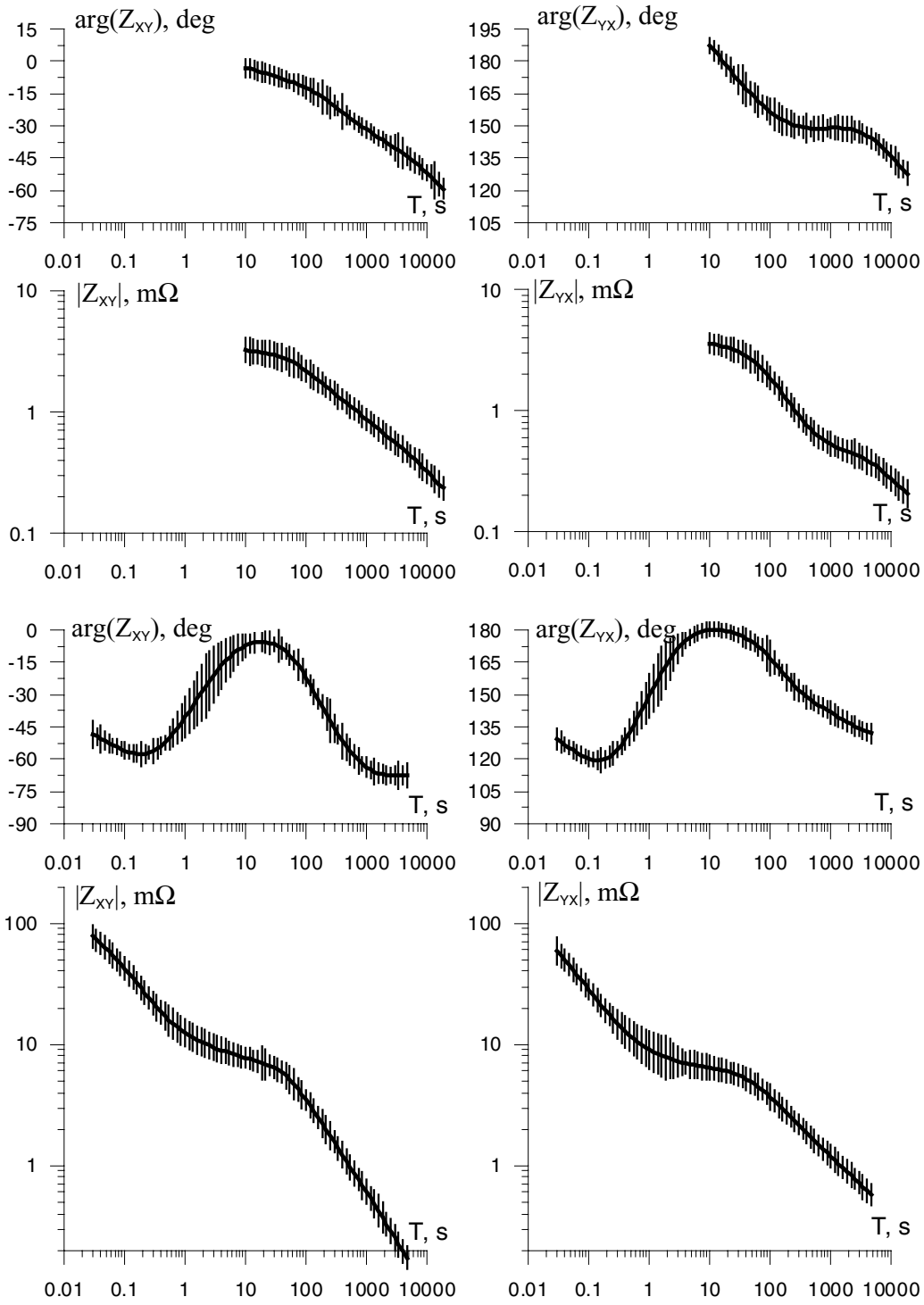

Figure 2. Impedance matrix components Zxy and Zyx for sites 01 (top) and 14 (bottom).

noise, primarily created by electrified railroads (Larsen *et al.* 1996; Aleksanova *et al.* 2003). We were not able to obtain impedance transfer functions at sites 07 and 08, located close to the LU–TESZ boundary. At the same time, tipper components, constructed using only magnetic fields, were estimated with high accuracy.

One way to evaluate the applicability of 1-D and 2-D approximations and the level of near-surface distortions is to consider the heterogeneity parameter N (Berdichevsky & Dmitriev 2002), the asymmetry parameter skew (Swift 1967) and the phase-sensitive asymmetry parameter η (Bahr 1988). We constructed these by using impedance components according to the following formulas:

$$N = \left|\sqrt{1 - 4\frac{Z_{XX}Z_{YY} - Z_{XY}Z_{YX}}{(Z_{XY} - Z_{YX})^2}}\right|, \quad \text{skew} = \left|\frac{Z_{XX} + Z_{YY}}{Z_{XY} - Z_{YX}}\right|,$$

$$\eta = \frac{\sqrt{\left|\text{Im}(Z_{XY}Z^*_{YY} + Z_{XX}Z^*_{YX})\right|}}{|Z_{XY} - Z_{YX}|},$$

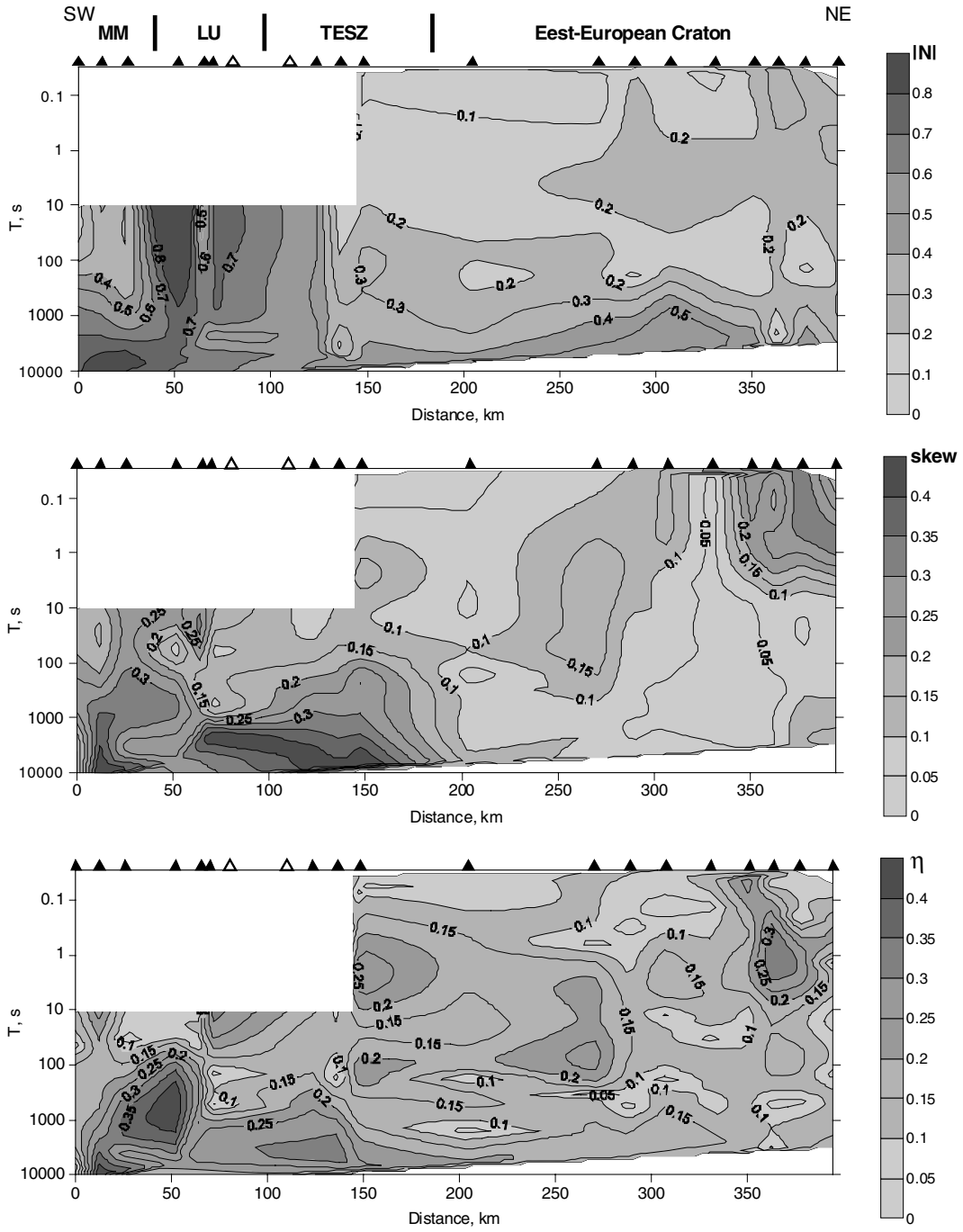

Figure 3. Pseudo-cross-sections of impedance invariants: inhomogeneity parameter N, asymmetry parameter skew, phase-sensitive asymmetry parameter η. Tectonic structures: MM, Malopolska Massif; LU, Lysogory Unit, TESZ, Trans-European Suture Zone.

where the asterisk means complex conjugation. These parameters are invariant to the rotation of the coordinate system. For the 1-D model, $Z_{XY} = -Z_{YX}$ and $Z_{XX} = Z_{YY} = 0$, therefore, $N = \text{skew} = \eta = 0$. For the 2-D model, we have $Z_{XY} \neq -Z_{YX}$ and $Z_{XX} = Z_{YY} = 0$ (in the principal directions), consequently $N \neq 0$, but skew $= \eta = 0$. If local near-surface 3-D inhomogeneities are superimposed on the regional 2-D background, then $N \neq 0$ and skew $\neq 0$, but $\eta = 0$. Finally, in the case of the model with regional 3-D inhomogeneities ($Z_{XY} \neq -Z_{YX}$ and $Z_{XX} + Z_{YY} \neq 0$) $N \neq 0$, skew $\neq 0$ and $\eta \neq 0$.

Pseudo-cross-sections of parameters N, skew and η are presented in Fig. 3 (note that we have short-period data only in the northeastern part of the profile). We see a striking difference between the southwestern 130 km and the remainder of the profile. In and near the LU, the N values are large. This is similar to the pattern for skew, especially at long periods. Increased η values correspond to the longest periods, in the LU they cover almost the whole period range and achieve a maximum. Obviously, 1-D approximation is not applicable here, and we could also have problems with a 2-D approach in the LU and at the long periods in the MM and southwestern TESZ.

In the northeastern TESZ and in the EEC all parameters have small values, indicating the absence of strong horizontal inhomogeneities. There are only two exceptions. First, at the longest periods

N has larger values. Second, increased values of all parameters are observed at rather short periods on the northeastern edge of the profile, where the Mazursko-Belarusian anticline is located. However, in general, 2-D approximation seems to be suitable and 1-D approximation is valid for short-period data in this part of the profile.

Concluding the heterogeneity and asymmetry parameters analysis, we can say there is a limited application for 1-D approaches (at short periods and with lower accuracy at long periods at the EEC), and 2-D structures seem to explain most of the impedance data, excluding LU and the adjacent sites. Through most of the profile the parameters change smoothly from site to site, evidence of the minimal influence of near-surface distortions. This is not true only at the LU, where near-surface inhomogeneities may be present.

These conclusions can be verified using impedance polar diagrams and induction arrows. Additionally, they will show the strike of the resistivity structures. Let us first consider impedance magnitude diagrams (Berdichevsky & Dmitriev 2002). In the 1-D case, the main impedance diagram is a circle and the additional impedance diagram contracts into a point. Above the 2-D medium, the main impedance diagrams are elongated along or across the strike and are symmetric with respect to these directions. The additional impedance diagram in the 2-D case consists of four equal leaves, zero additional impedance values correspond to directions along and across the strike. The impedance magnitude diagrams along our profile are presented in Fig. 4. At the EEC, the main impedance diagrams are weakly elongated, especially at short periods, and additional impedance diagrams are small. The diagrams slowly vary along the profile, confirming the absence of strong local

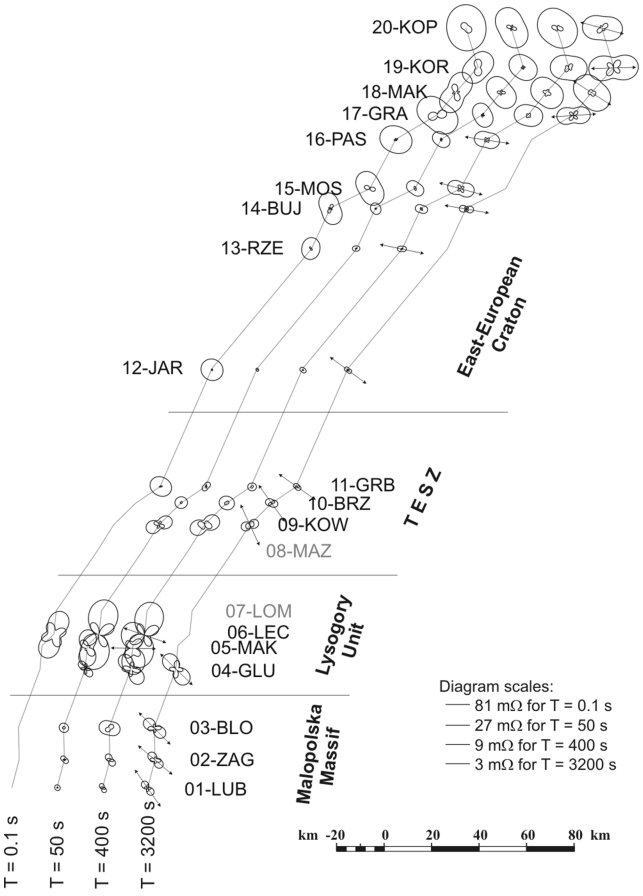

Figure 4. Map of impedance magnitude polar diagrams.

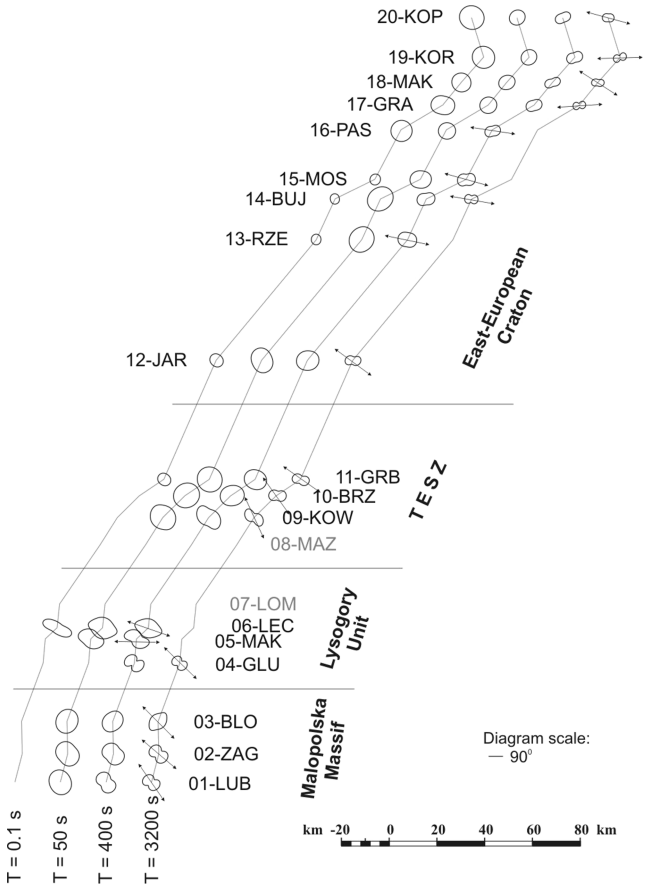

Figure 5. Map of impedance phase polar diagrams.

distortions. In the southwest, most of the main impedance diagrams are strongly asymmetric and additional impedance diagrams are large. At some sites the diagrams are period-dependent but at others they are not. Sometimes their form and orientation do not change from site to site, but at several sites they become essentially different. This complex behaviour probably reflects the influence of both near-surface and larger-scale 3-D inhomogeneities.

Fig. 5 presents impedance phase diagrams. In the 1-D case such diagrams are circles, and for the 2-D medium they stretch along or across the strike of the structures. At most of the sites the diagrams differ from a circle as the period increases. In the southwest, they sometimes abruptly vary from site to site, while at the EEC such variations are small. In the MM, LU and partly TESZ, the phase diagrams are primarily elongated in the northwestern or northeastern directions. At the EEC, the direction of the long axis of the diagrams is between northeast and east. The behaviour of the phase diagrams is close to that of the main impedance magnitude diagrams.

Polar diagrams, being generally elongated across or along the profile, allow us to assume that 2-D interpretation is possible. Low manifestation of near-surface distortions (except for LU) means it is not necessary to apply data normalization or decomposition.

For further 2-D inversion we need to select the principal directions (Swift 1967; Eggers 1982; Bahr 1988; Groom & Bailey 1989). We understand them as the directions in which additional (minor) impedance components vanish. It is important that apparent resistivity can be calculated with no ambiguity in these directions, because formulas obtained, for example, for isotropic and anisotropic half-spaces, coincide in this case (Semenov 2000).

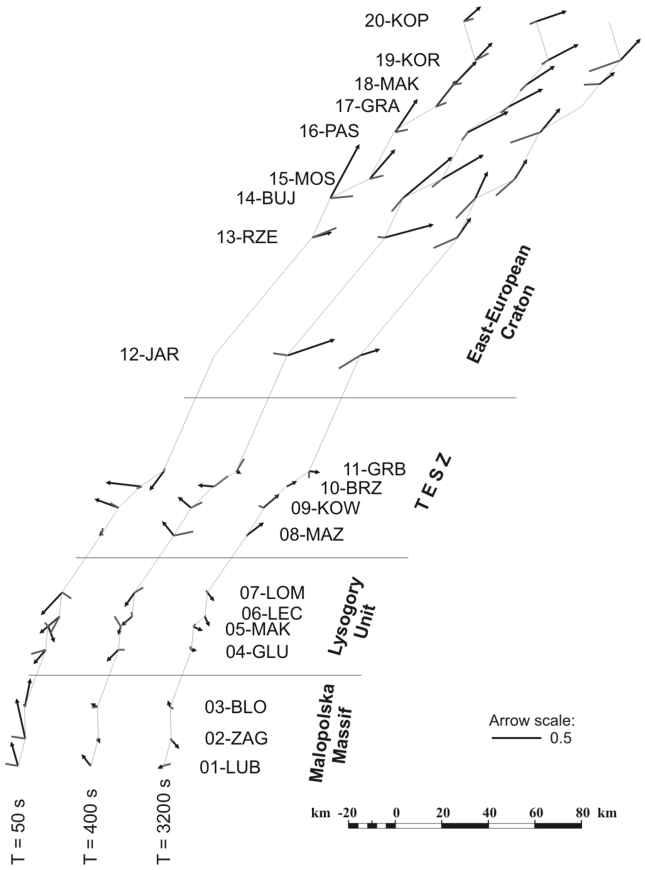

Figure 6. Map of induction arrows at three periods. Real induction arrows ended with triangles, imaginary ones have no ending.

The principal directions of impedance matrix were selected using the minima of the additional impedance polar diagrams at the largest period and used for shorter periods as well. One of them, roughly perpendicular to the profile and parallel to resistivity structures, is considered as quasi-longitudinal, and the other one, roughly parallel to the profile and perpendicular to the structures is considered as quasi-transversal. Quasi-longitudinal directions are presented in Figs 4 and 5. They coincide well with one of the main impedance diagram axes and with one of the phase polar diagram axes.

Fig. 6 presents the map of induction arrows. Real induction arrows show the direction from conductive to resistive structures (so-called Wiese convention). Imaginary induction arrows are collinear with them, in the case of the 2-D medium. In the MM at long periods, induction arrows are small and their direction is chaotic. In the LU they do not increase but the orientation of real induction arrows becomes regular and they mostly point south. In the TESZ at short periods, they point west, but at long periods they are mostly oriented northeast and are also very small. At the EEC, real induction arrows are large and oriented towards the northeast. As at most of the sites, real induction arrows run approximately along the profile and the imaginary ones are roughly collinear to them, the induction arrows provide evidence for the predominant influence of 2-D regional structures. It seems that in our case tipper satisfies 2-D approximation better than impedance.

2-D modelling provides transfer functions in two directions—longitudinal and transversal to structures; it is also assumed that the profile is orthogonal to their strike. To obtain transfer functions for the 2-D interpretation, we rotated the impedance matrix to match the selected principal directions. We also projected induction arrows to the profile azimuth, which is about 30° clockwise for the 11 southwestern sites and 40° for the nine northeastern sites.

After the rotation we obtain three complex transfer functions for further analysis. The first one is quasi-transversal impedance Z^{TM}, corresponding to currents flowing across the structures (it includes transverse electric and longitudinal magnetic field). The others are quasi-longitudinal impedance Z^{TE} and tipper W^{TE}, both corresponding to currents flowing along the structures (and including longitudinal electric field, transverse and vertical magnetic field). We consider simple transformations of $|Z^{\mathrm{TM}}|$ and $|Z^{\mathrm{TE}}|$—apparent resistivities $\rho^{\mathrm{TM}} = |Z^{\mathrm{TM}}|^2/(\omega \cdot \mu_0)$ and $\rho^{\mathrm{TE}} = |Z^{\mathrm{TE}}|^2/(\omega \cdot \mu_0)$, impedance phases $\varphi^{\mathrm{TM}} = \mathrm{Arg}\,(Z^{\mathrm{TM}})$ and $\varphi^{\mathrm{TE}} = \mathrm{Arg}\,(Z^{\mathrm{TE}})$, the real and imaginary part of tipper Re (W^{TE}) and Im (W^{TE}). Pseudo-cross-sections of $\rho^{\mathrm{TM}}, \varphi^{\mathrm{TM}}, \rho^{\mathrm{TE}}, \varphi^{\mathrm{TE}}$, Re (W^{TE}) and Im(W^{TE}) are presented in Figs 7–9.

Apparent resistivities ρ^{TM} and ρ^{TE} (Figs 7 and 8) generally increase from short to longer periods showing a transition from sediments to consolidated crust. The impedance phases φ^{TM} and φ^{TE}, after a short increase, decreases at large periods, being sensitive to a reduced resistivity of the lower crust and/or upper mantle. The lowest values of ρ^{TM} and ρ^{TE} are observed in the southwest of the EEC, and two anomalies of increased values correspond to the LU and the Mazursko-Belarusian anticline. Variations of apparent resistivities and phases from site to site are slow, except the southwestern part of the profile, especially in the mountains.

A strong anomaly of the real part of tipper Re (W^{TE}) is observed at the EEC (Fig. 9). Here Re (W^{TE}) values exceed $+0.4$, and at one site reach $+0.7$. These maximal values correspond to a period of approximately 300 s. In the southwestern part of the profile, only small local anomalies of Re (W^{TE}) are present. The values of the imaginary part of tipper Im (W^{TE}) are smaller, not exceeding ± 0.3. In the northeast, zero values of Im (W^{TE}) obviously correspond to the Re (W^{TE}) maximum.

Typical transfer functions are shown in Fig. 10. They correspond to site 02, situated in the MM, and site 15, which is at the EEC. At site 02, quasi-transversal and quasi-longitudinal impedance phases and apparent resistivities are essentially different, Re (W^{TE}) and Im (W^{TE}) values are rather small, especially at large periods. Site 15 is characterized by similar TM and TE curves and large tipper values.

DATA INVERSION

The reliable information about resistivity structures can be incorporated into a prior model to be used in the 2-D inversion. Our prior model includes near-surface conductive structures, the homogeneous crust with Carpathian conductivity anomaly, and the upper mantle with resistivity varying in the vertical direction (Fig. 11).

Resistivity variations with depth in the upper mantle was determined as a result of interpretation of the combined curves of MT and magnetovariational (MV) soundings performed in observatories. The following parameters, applicable for the survey area, are used: resistivity $\rho = 400\,\Omega$ m down to 150 km depth, $\rho = 25\,\Omega$m to 210 km, $\rho = 100\,\Omega$m to 420 km, $\rho = 10\,\Omega$m to 670 km, $0.5\,\Omega$m below that (Semenov *et al.* 1998).

Subsurface sediments essentially influence long-period data, and we inserted them into our model to separate the effects of near-surface and deep anomalies. Sedimentary structures can be studied using short-period MT data. Data analysis showed that we can interpret it applying the 1-D approach. We use a layered inversion code to fit the short-period determinant apparent resistivity and

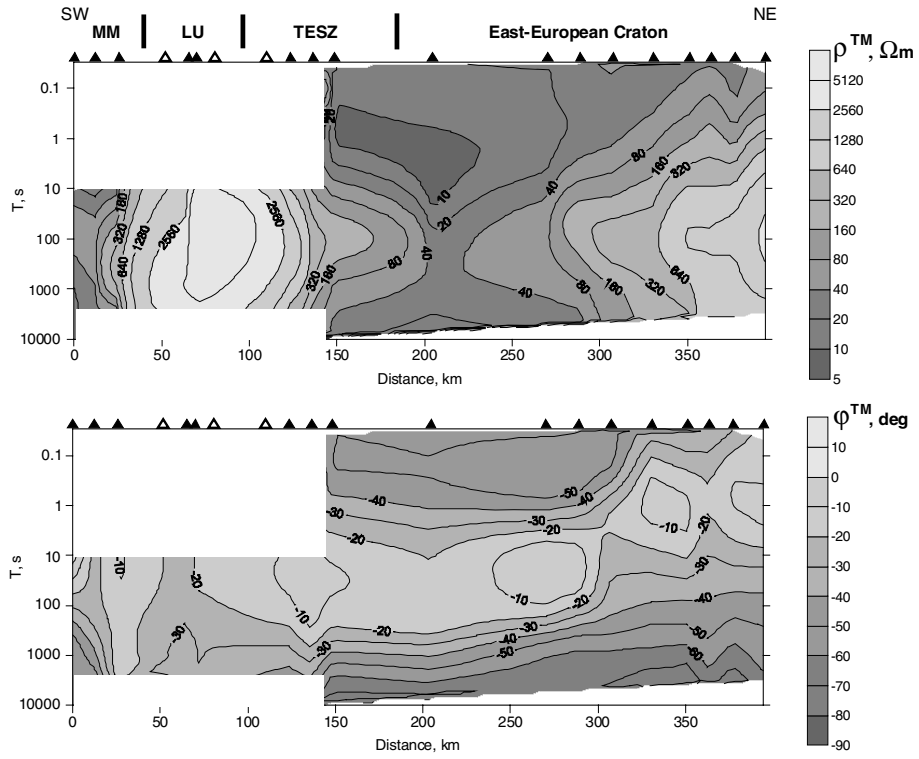

Figure 7. Pseudo-cross-sections of observed transverse apparent resistivity and impedance phase.

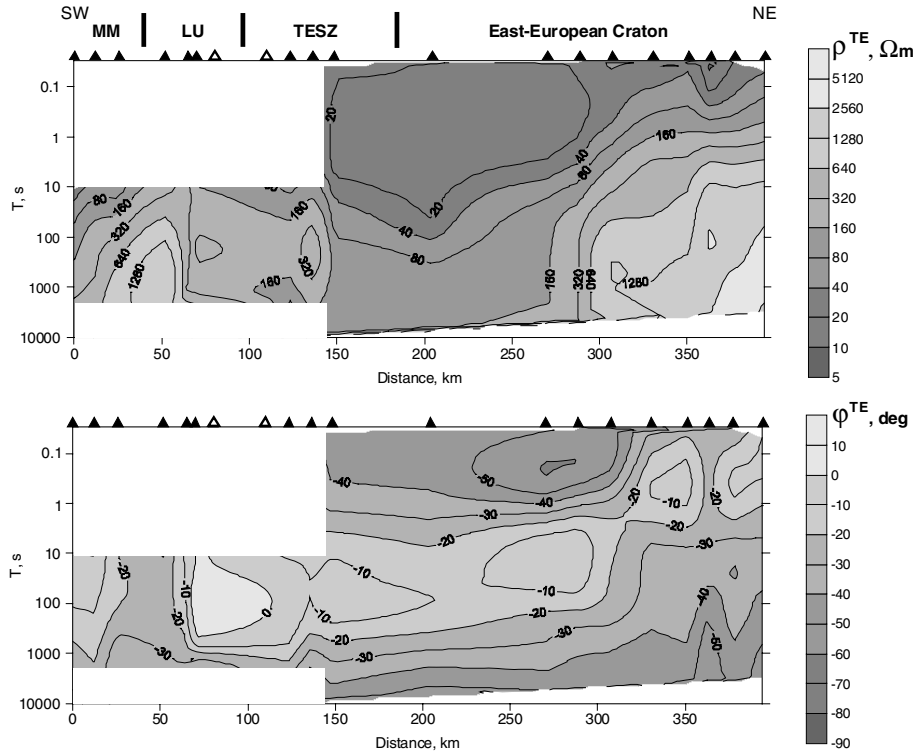

Figure 8. Pseudo-cross-sections of observed longitudinal apparent resistivity and impedance phase.

impedance phase curves: $\rho^{\det} = |Z^{\det}|^2/(\omega \cdot \mu_0)$, $\varphi^{\det} = \mathrm{Arg}\,(Z^{\det})$, where $Z^{\det} = \sqrt{Z_{XX} \cdot Z_{YY} - Z_{XY} \cdot Z_{YX}}$ (Berdichevsky & Dmitriev 2002). At the EEC, the thickness of the sediments is well known (Znosko 1998) and was used as the constraint during the inversion. The result is incorporated into the prior model, which is shown in Fig. 11 together with the graph of sediments conductance S. At the EEC, the sediments are described by two layers, the lower one having a lower resistivity. Two more layers were added in the zone of

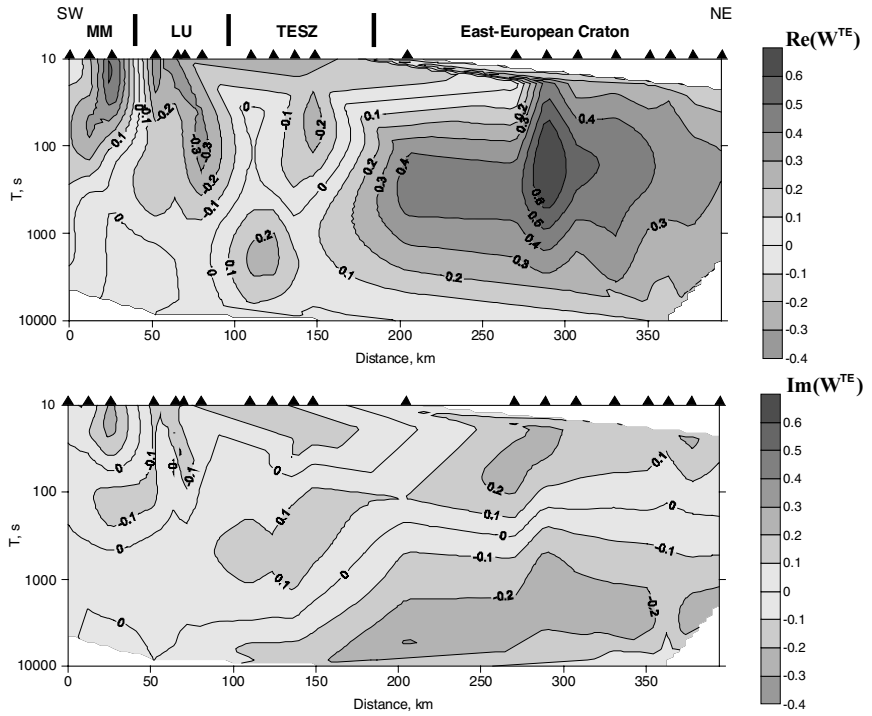

Figure 9. Pseudo-cross-sections of observed real and imaginary parts of tipper.

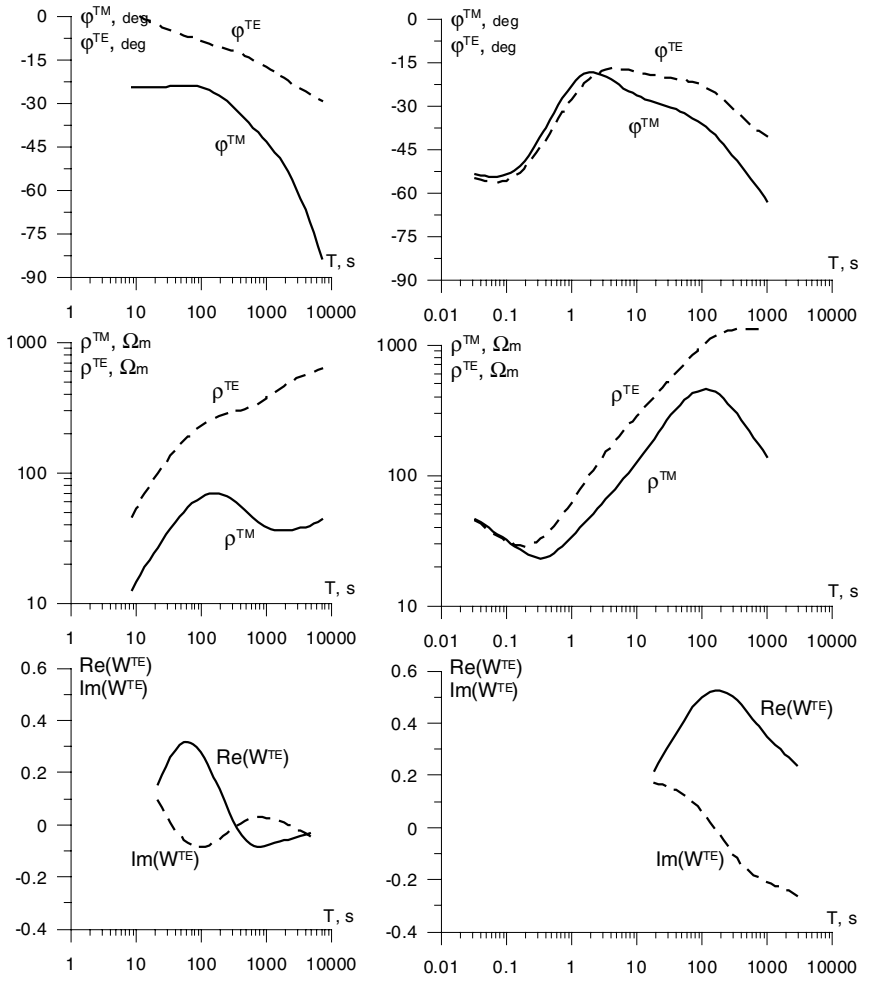

Figure 10. Transverse and longitudinal impedance phases and apparent resistivities, real and imaginary parts of tipper. Sites 02 (left) and 15 (right).

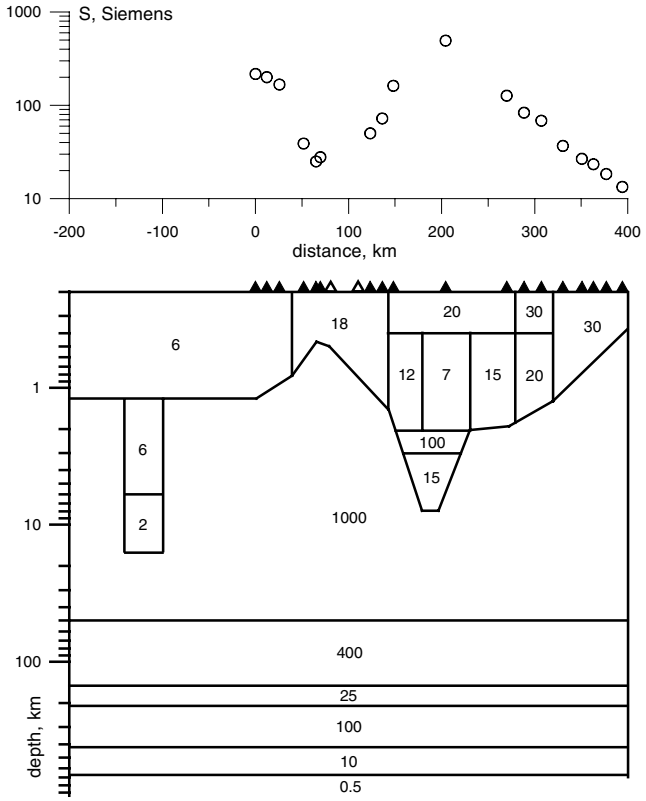

Figure 11. Prior resistivity model (below) and graph of sediments conductance (above). The values of resistivity are indicated in Ωm.

maximal conductance. In the southwestern part of the profile we do not have high-frequency data, and near-surface conductive rocks are described by one layer.

The Carpathian conductivity anomaly, responsible for the large induction arrows radiating from it, is situated in the south, outside of the profile (Jankowski 1967; Rokityanskiy *et al.* 1975; Jankowski *et al.* 1985; Ernst *et al.* 2002). Strangely, we do not observe large induction arrows in the southern part of our profile. However, this situation is not typical for Carpathian surroundings, and therefore, does not mean the absence of the Carpathian anomaly's influence. It can be explained by the presence of conductive anomaly inside the profile, compensating this influence.

For the 2-D interpretation we use ρ^{TM}, ρ^{TE}, φ^{TM}, φ^{TE}, Re (W^{TE}) and Im (W^{TE}) in the period range between 1 and 10 000 s. As this may not allow us to study the asthenosphere without ambiguity, we supplement these data with long period curves of deep soundings, performed at the observatories. We use the results, obtained at the nearest observatories HRB (Hurbanovo, Slovakia), BEL (Belsk, Poland) and MNK (Minsk, Belarus). Results obtained at HRB were added to data from site 01, at BEL—to data from sites 10 and 11, at MNK—to data from site 20, so between these sites horizontal variations of deep resistivity structure were possible. For each deep sounding only one apparent resistivity and one impedance phase long-period curve can be derived because of the source of initial magnetic field (Fujii & Schultz 2002). These curves correspond to local geomagnetic longitude for Dst variations and are not attributed to any direction for Sq variations, being considered as effective responses (Semenov & Jozwiak 2005). During the inversion we use them as longitudinal curves and give them large weights to make the ρ^{TE} and φ^{TE} model responses approach them as the periods increase.

The data components (quasi-transversal impedance Z^{TM}, quasi-longitudinal impedance Z^{TE}, tipper W^{TE}) may significantly differ in sensitivity to resistive and conductive structures, in robustness to 3-D distortions, and even in tolerance to industrial electromagnetic noise. It is important to take this into account during interpretation. As discussed before, in our case the tipper data are of good quality and satisfies the 2-D approximation well. It also has high sensitivity to conductive inhomogeneities. Therefore, we give greater priority to W^{TE}. However, it is less sensitive to subhorizontal structures. In order to obtain a resistivity model with a more or less properly layered structure we need to use impedance data, which have higher sensitivity to vertical variations of resistivity. Unfortunately, as stated above, the impedance data quality is lower and 3-D distortions are present at some sites. Thus, we treat Z^{TM} and Z^{TE} with less confidence (especially the latter, as 2-D modelling cannot explain its galvanic distortions), and primarily to roughly control the layered structure.

We use two types of software for 2-D data interpretation. First, we apply the smoothed-structure inversion code REBOCC (Siripunvaraporn & Egbert 2000) to reveal major resistivity anomalies. Then we move on to a program working with piecewise-uniform models, which is a convenient tool for introducing details and making the resistivity model compatible with geological and other geophysical data (Wieladek *et al.* 1981; Nowozynski & Pushkarev 2001).

The REBOCC software constructs a resistivity model which is consistent with observed data and the prior model and which has smooth variations of resistivity. Note that no resistivities were fixed, so all the prior structures were corrected during the inversion. Separate inversions of different data components were performed first (observatory data were also used in each inversion). We were unable to obtain small misfit and a plausible model inverting Z^{TE}, probably because of its galvanic distortions (in particular, distortions developed only in low-frequency range, and therefore, significantly modifying the shapes of apparent resistivity curves). The results of separate inversions of Z^{TM} and W^{TE} using the prior model considered above are presented in Fig. 12 (cross-sections of the shallow and deep parts of both models are shown). The misfit is characterized by rms $= 2.4$ for Z^{TM} and rms $= 0.7$ for W^{TE}. Some features are common to both results: that the EEC has the most resistive lithosphere and the conductivity at 150–200 km depth beneath the edge of the EEC is large but decreases to northeast. The most striking difference between these two models occurs with respect to the crust of the LU. It is resistive according to Z^{TM}, probably because of high sensitivity of this component to resistive structures and low sensitivity to isolated local conductive structures. The sensitivity of W^{TE} is just the opposite and the inversion result demonstrates this perfectly. W^{TE} revealed a small conductive structure beneath the LU and a deeper one closer to the southeast, however together they can be considered as parts of an inclined and rather thin structure.

We also performed a joint inversion of Z^{TM} and W^{TE} data, giving the tipper values a larger weight. The resulting cross-section is presented in Fig. 13, the corresponding rms $= 1.6$. The model includes a conductive anomaly mainly at crustal depth in the northeastern part of the LU. This was also revealed by separate W^{TE} inversion, but now it appears as a single subvertical structure, possibly because of greater smoothing. Another anomalous zone, although less evident, can be found at the EEC. Here the near-surface conductance increased between 250 and 300 km of the profile, and a deep low resistivity zone is also present. These features can also be seen on the cross-sections obtained during separate inversions of Z^{TM} and W^{TE}. It is also clearly seen that the conductivity at 150–200 km

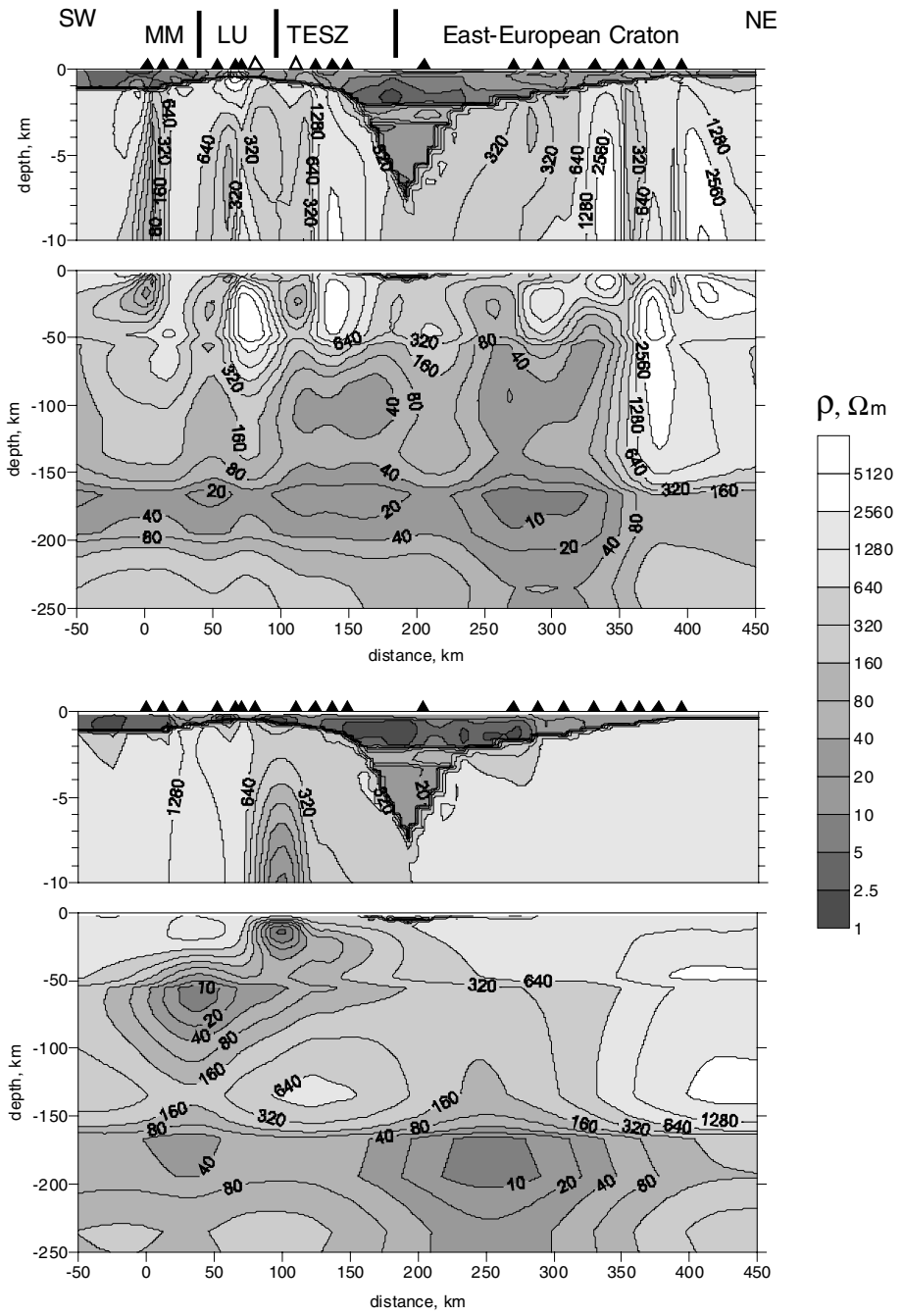

Figure 12. Result of REBOCC inversion of transverse impedance (above) and tipper (below).

depth beneath the northeastern part of the profile is smaller, than beneath the other structures.

REBOCC inversion allowed us to reveal major anomalies in the crust and upper mantle. Using this information, we applied interactive 2-D interpretational software, based on piecewise-uniform resistivity distribution (Nowozynski & Pushkarev 2001), to obtain a cross-section which is more detailed and more realistic from a geological point of view. At this stage, the major anomalies revealed by REBOCC inversion were approximated by rectangular blocks, and added to the structures of the starting model, presented in Fig. 11. This blocky model was manually adjusted (mainly using forward modelling function) in order to fit all the data (W^{TM}, Z^{TM} and Z^{TE}) as far as possible, and at the same time to comply with the geological information. The result is presented in Fig. 14 (note that the vertical scale changes at 10 km). We would like to emphasize, that although this resistivity model is more detailed, than REBOCC inversion results, it includes only blocks, which influence the model response significantly.

The corresponding pseudo-cross-sections, showing the residuals between observed and modelled data, are presented in Figs 15–17. The misfit is small for tipper components, as they were given the greatest priority. Only high-frequency data, especially in the southwest, and a small long-period anomaly at the TESZ cause some discrepancy. The data fit is generally not bad for transverse apparent resistivity data, at least there are no large zones of systematic discrepancies between model and experiment. It is worse for

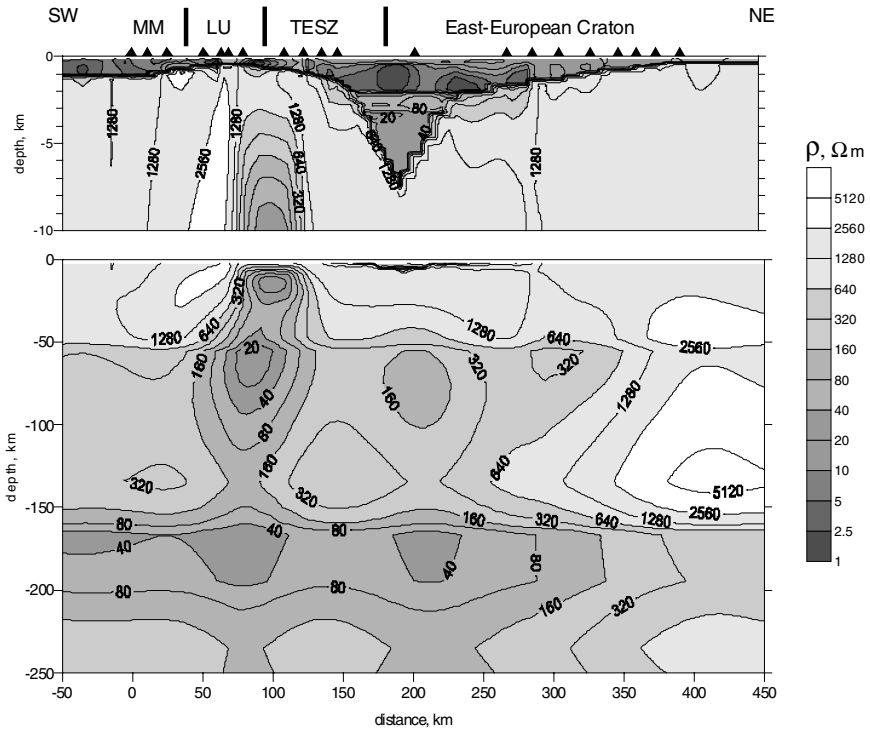

Figure 13. Result of simultaneous REBOCC inversion of transverse impedance and tipper.

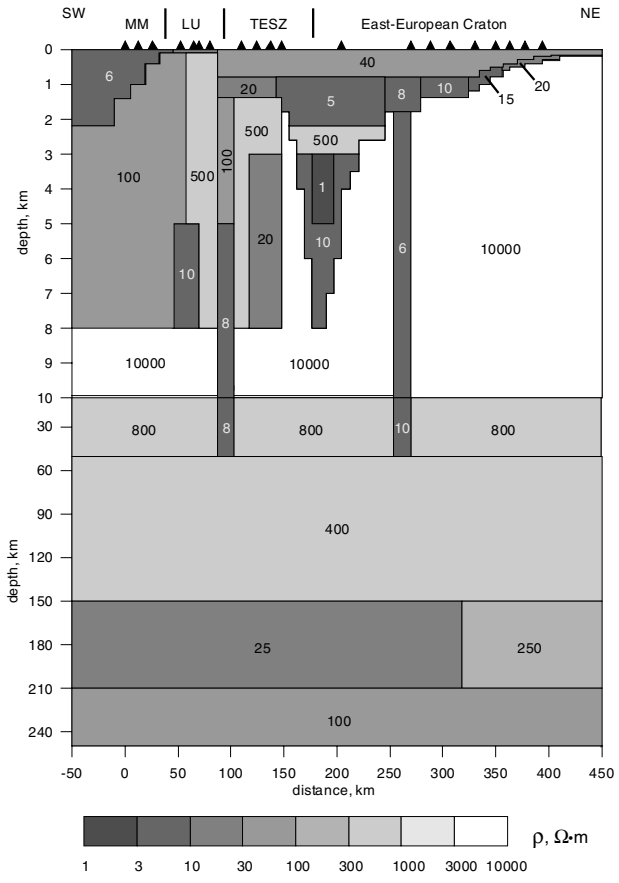

Figure 14. Final blocky resistivity cross-section along the profile.

the transverse phase and especially for longitudinal impedance, the latter probably because of 3-D galvanic distortions. The model is in good agreement with long-period geomagnetic observatory data (Fig. 18), allowing to suppose that the estimation of upper-mantle conductivity is reliable.

DISCUSSION AND CONCLUSIONS

Let us consider the resulting resistivity cross-section along the profile (Fig. 14) in detail. The Carpathian anomaly is present in our model but not shown, as it is situated outside the profile. As low-frequency electromagnetic field generally does not allow estimating the positions of resistivity boundaries with high precision (as boundary positions in the seismic method), the model is schematic and the blocks have rectangular shapes. It should be understood that sharp boundaries between resistivity blocks stem from numerical modelling techniques and should not be interpreted directly in terms of geological units.

The shallow part of the model in the southwest is formed by conductive sediments of MM. Below them there are some more resistive metamorphic rocks with their lower boundary at 8 km depth. Beneath the LU, these rocks are characterized by a more complicated structure. The southwestern part of the LU is more conductive than the northeastern section, especially in the depth range of about 5–8 km. This can be explained by different though largely unknown factors, such as differences in petrologic composition, water content, metamorphism, or different bedding of anisotropic rocks (e.g. subhorizontal in the southwest and subvertical in the northeast). A deep conductive fault is present in the northeastern LU (known as the Holy Cross fault), its low resistivity being evidence that it is graphitized or fluid-saturated, or both. Beneath the TESZ, at the depth of 3–8 km, low resistivity complex of presumably sedimentary rocks may be identified. These structures are also present in the resistivity

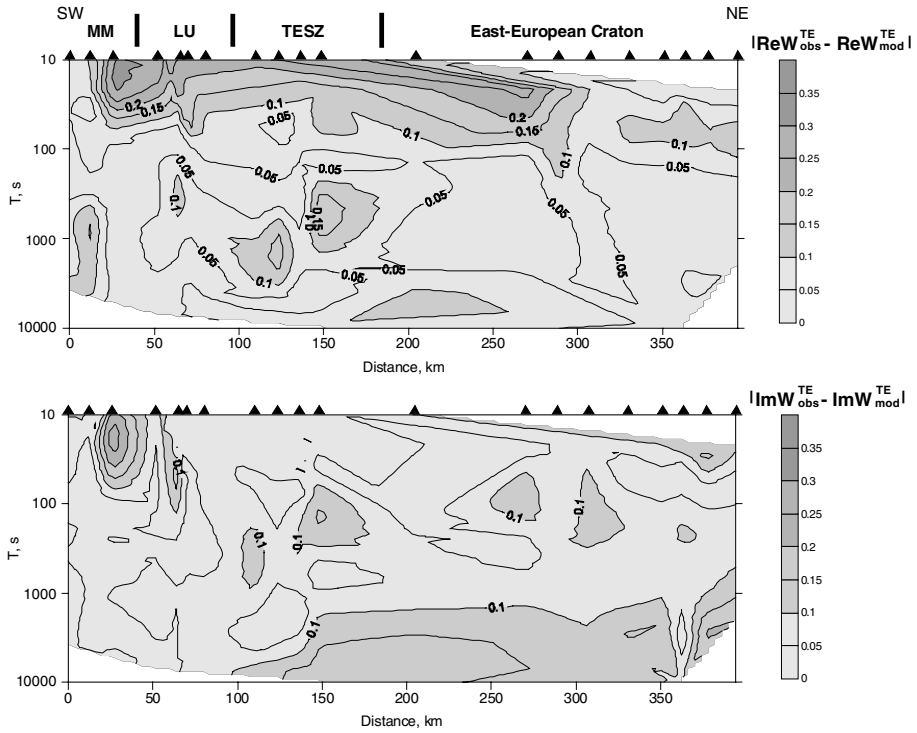

Figure 15. Pseudo-cross-sections of tipper data misfit.

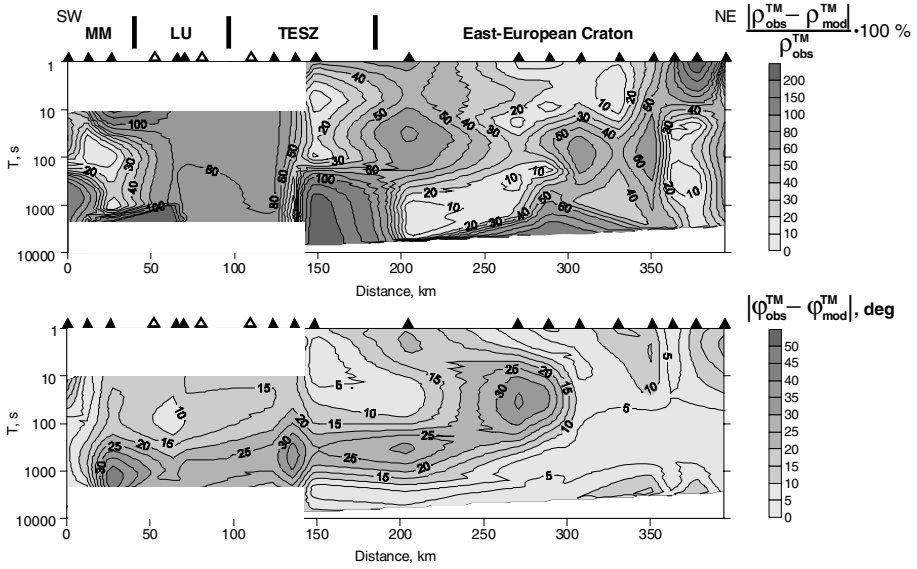

Figure 16. Pseudo-cross-sections of transverse impedance data misfit.

model, previously constructed using only data from 10 southwestern sites (Semenov *et al.* 1998).

Further to the northeast, tectonic structure becomes less complicated, the thickness of the sediments is better known from previous geological and geophysical studies (Znosko 1998), and therefore, this thickness is given with more details. Between 160 and 220 km of the profile there is a Lublin trough, presumably filled with Silurian-Carboniferous sediments. The very low resistivity of its central part can theoretically be explained by a high content of mineralized water or graphite, but it should be treated with less confidence, as its presence is necessary to fit the data at only one solitary site. These rocks are covered by Permian-Cretaceous sediments that stretch far inside the EEC. They consist of two layers, the lower being more conductive probably because it is saturated with mineralized water.

Between 250 and 270 km of the profile we introduce a deep subvertical crustal anomaly, which can be interpreted as a fault zone. Unlike the one in the northeast part of the LU, this one was not well imaged by the REBOCC inversion. However, a model with this feature provides a better data fit and allows us to avoid inserting small and very conductive geological bodies within the sediments (Fig. 13), which might be difficult to explain from a geological point of view. Deep conductive faults are typical to TESZ, two are

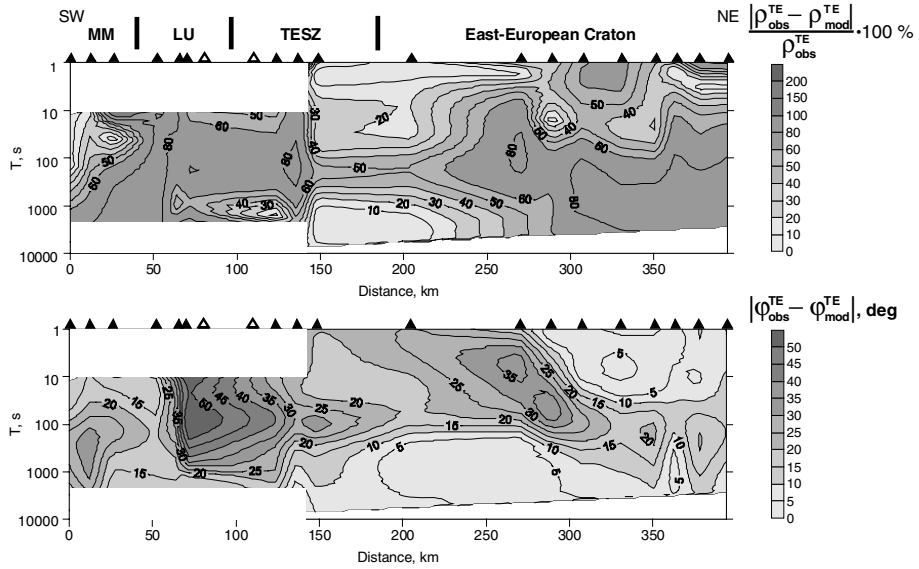

Figure 17. Pseudo-cross-sections of longitudinal impedance data misfit.

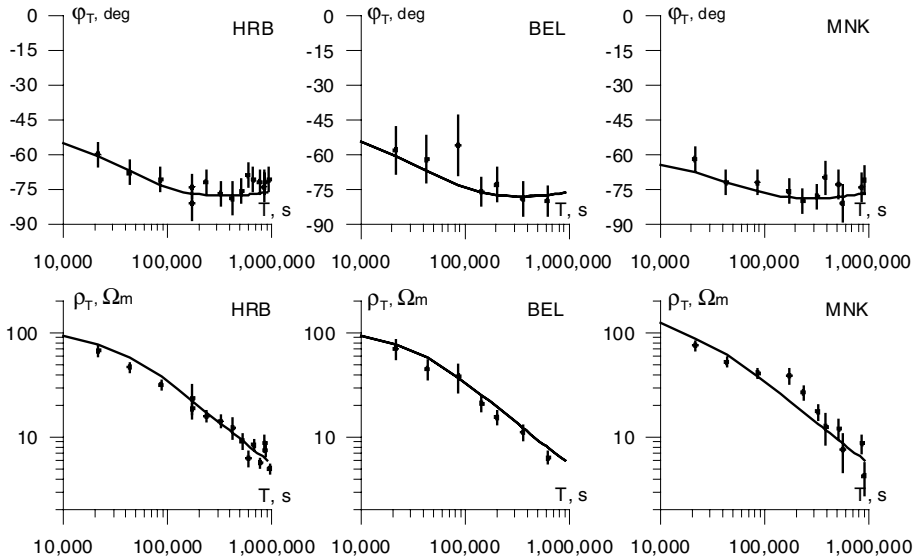

Figure 18. Comparison of modelled long-period responses (solid lines) with geomagnetic observatory data. Left—response for site 01 compared with Hurbanovo observatory data, centre—sites 10 and 11 with Belsk, right—site 20 with Minsk.

proposed to occur in southeast Poland (Ernst *et al.* 2002), and one is reported in Sweden (Smirnov & Pedersen 2005). However, a different way of interpretation of the considered conductive anomaly may be possible, as there is no certain evidence for presence of fault here in other geological and geophysical data.

The underlying upper crust may be considered consolidated, since it has a resistivity of the order of 10 000 Ωm, which is in accordance with the estimates for Belarus (Fainberg *et al.* 1998), which is close to the northeastern end of our profile. Below 10 km the resistivity gradually decreases. Two fractures penetrate through the crust down to 50 km depth. In the upper mantle at approximately 150–210 km depth, the resistivity significantly increases beneath the EEC. The upper-mantle conductance increase from the EEC to TESZ had been conjectured before using data from the 10 northeastern sites (Semenov *et al.* 2002). And in a study based on data from 10 southwestern sites, a conductive anomaly in the lower crust was considered beneath the TESZ instead of the laterally inhomogeneous mantle, probably because of insufficient data at the opposite side of the TESZ (Semenov *et al.* 1998).

It is important to make sure that the response of the revealed conductivity anomalies is significant. We performed several sensitivity tests, some results are presented in Figs 19 and 20. The former figure presents observed and modelled Re (W^{TE}) values at 136 s periods. Dashed curves show how the modelled data changes if we remove the deep fault at the boundary between LU and TESZ or at the EEC (increase their resistivity to 1000 Ωm). Obviously the data fit becomes much worse if we remove one of these conductive features. Another important part of our model is the increase of resistivity at the EEC in the 150–210 km depth range. Fig 20 presents observed and modelled Re (W^{TE}) data at 1166 s period. If we continue the 25 Ωm upper-mantle layer beneath the EEC, the data fit in the northeastern part of the profile becomes essentially worse.

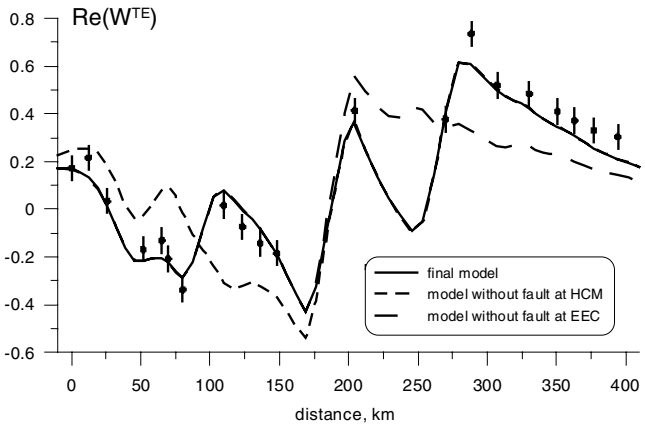

Figure 19. Real tipper component Re (W^{TE}) at period 136 s. Black dots with bars—observed data.

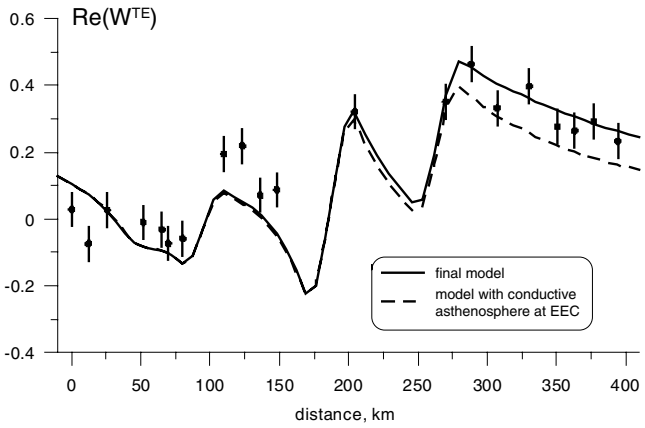

Figure 20. Real tipper component Re (W^{TE}) at period 1166 s. Black dots with bars—observed data.

Comparing the discussed resistivity model (Fig. 14) with the seismic results obtained along the profile C01 of the CELEBRATION project (Sroda *et al.* 2006), roughly coinciding with our profile, we see some common features. The conductive depression between 160 and 220 km appears as a low-velocity (5.20 km s^{-1}) zone. Below it, between deep conductive faults, there is a high-velocity (7.15 km s^{-1}) anomaly, reaching 30 km depth. A wide low-velocity (5.85 km s^{-1}) zone is present beneath the LU, but it reaches 20 km. The Moho boundary is at 40 km depth at the EEC and TESZ and goes up to 30 km at the MM, but we do not see it in our model as this boundary does not have contrasting in resistivity. The asthenosphere depth is not reached by the CELEBRATION study. However, as discussed in the introduction, deep seismic tomography data allowed us to estimate that *S*-wave velocities in the upper mantle are higher beneath the EEC than at the Phanerozoic Europe (Zielhuis & Nolet 1994). And geothermal modelling shows that temperature beneath the EEC is lower, especially at upper-mantle depths (Majorowicz 2004). Although a resistivity increase at 150–210 km depth is introduced in our model, this can be interpreted both as the decrease of the asthenosphere conductance or its dipping. The latter does not contradict the seismic data, indicating that the thickness of the continental lithosphere can reach 250 km (Gung *et al.* 2003).

ACKNOWLEDGMENTS

Data acquisition and processing was conducted thanks to support from the Polish Committee for Scientific Research (grants PB0854/S6/94/06, 6P04D 01220, 6P04D 03512 and 9T12B 025 15). The first author was supported by INTAS (grant 03-55-2126).

We thank two anonymous reviewers for their helpful comments and suggestions.

REFERENCES

Aleksanova, E.D., Kulikov, V.A., Pushkarev, P.Yu. & Yakovlev, A.G., 2003. Ispolzovanie poley elictrifitsirovannyh zheleznyh dorog pri provedenii elektromagnitnyh zondirovaniy (The application of electromagnetic fields created by railroads for electromagnetic sounding). Geologiya i Razvedka (Geology and Prospecting), 2003, No. 4, pp. 60–64 (in Russian).

Bahr, K., 1988. Interpretation of magnetotelluric impedance tensor: regional induction and local telluric distortion, *J. Geophys.,* **62,** 119–127.

Berdichevsky, M.N. & Dmitriev, V.I., 2002. *Magnetotellurics in the Context of the Theory of Ill-Posed Problems*, SEG, Tulsa, 215 p.

Dadlez, R., Kowalczewski, Z. & Znosko, J., 1994. Some key problems of the Permian tectonics of Poland, *Geol. Quart.,* **38,** 29–189.

Eggers, D.E., 1982. An eigenstate formulation of the magnetotelluric impedance tensor, *Geophysics,* **47,** 1204–1214.

Ernst, T. et al., 1997. Electromagnetic soundings across the Tatra mountains, *Acta Geophys. Pol.,* **45**(1), 33–44.

Ernst, T., Jankowski, J., Jozwiak, W., Lefeld, J. & Logvinov, I., 2002. Geoelectrical model along a profile across the Tornquist-Teisseyre zone in south-eastern Poland, *Acta Geophys. Pol.,* **50**(4), 505–515.

Fainberg, E.B. et al., 1998. Deep electromagnetic Soundings in Belarus: Europrobe Crustal Soundings, *Phys. Solid Earth,* **34**(6), 486–495.

Fujii, I. & Schultz, A., 2002. The 3D electromagnetic response of the Earth to ring current and auroral oval excitation, *Geophys. J. Int.,* **151**(3), 689–709.

Gung, Y., Panning, M. & Romanowicz, B., 2003. Global anisotropy and the thickness of continents, *Nature,* **422,** 707–711.

Gordienko, V.V. & Zavgorodnaya, O.V., 1996. Estimation of heat flow in Poland, *Acta Geophys. Pol.,* **44**(2), 173–180.

Grabowska, T. & Bojdys, G., 2001. The border of the East-European craton in south-eastern Poland based on gravity and magnetic data, *TerraNova,* **13**(2), 92–98.

Grad, M., Guterch, A. & Mazur, S., 2003. Seismic refraction evidence for crustal structure in the central part of the Trans-European Suture Zone in Poland, in *Paleozoic Amalgamation of Central Europe*, Vol. 201, pp. 295–309, eds Winchester J.A., Pharaoh, T.C. & Verniers J., Geological Society, London.

Groom, R.W. & Bailey, R.C., 1989. Decomposition of magnetotelluric impedance tensor in the presence of local three-dimensional galvanic distortion, *J. geophys. Res.,* **94**(B2), 1913–1925.

Guterch, A., Grad, M., Thybo, H., Keller, G.R. & POLONAISE Working Group, 1999. POLONAISE'97—an international seismic experiment between Precambrian and Variscan Europe in Poland, *Tectonophysics,* **314,** 101–121.

Guterch, A., Grad, M., Keller, G.R. & CELEBRATION, Organizing Committee, 2001. Seismologists Celebrate the new Millennium with an experiment in Central Europe, *EOS Transactions,* **82**(45), 529, 534–535.

Jankowski, J., 1965. Short-period variations of the Earth's magnetic field on the territory of Poland and their relation to deep substratum structure, *Acta Geophys. Pol.,* **13**(2), 85–105.

Jankowski, J., 1967. The marginal structure of the East European platform in Poland on the basis of data on geomagnetic field variations, *Publ. Inst. Geophys. Pol. Acad. Sc.,* **14,** 93–102.

Jankowski, J., Tarlowski, Z., Praus, O., Pecova, J. & Petr, V., 1985. The results of deep geomagnetic soundings in the west Carpathians, *Geophys. J. R. astr. Soc.,* **80,** 561–574.

Jankowski, J., Ernst, T. & Jozwiak, W., 2004. Effect of the near-surface layer on the geomagnetic induction arrows: an example from the East European platform, *Acta Geophys. Pol.,* **52**(3), 349–361.

Keller, G.R. & Hatcher, R.D., 1999. Some comparisons of the structure and evolution of the southern Appalachian-Ouachita orogen and portions of the Trans-European Suture Zone region, *Tectonophysics,* **314**, 43–68.

Krolikowski, C., Petecki, Z., Jacyna, I., Korabliova, L. & Nasedkin, V., 1999. Gravity and magnetic maps in the Polish-Lithuanian cross-border area, PGI, Warsaw.

Larsen, J.C., Mackie, R.L., Manzella, A., Fiordelisi, A. & Rieven, S., 1996. Robust smooth magnetotelluric transfer functions, *Geophys. J. Int.,* **124,** 801–819.

Majorowicz, J.A., 2004. Thermal lithosphere across the Trans-European suture zone in Poland, *Geol. Quart.,* **48,** 1–14.

Marianiuk, J., 1977. Photoelectric converter for recording the geomagnetic field elements: construction and principle of operation, *Publ. Inst. Geophys. Pol. Acad. Sci.,* C-4(114), 57–73.

Marianiuk, J., 2000. Induction Magnetometers for Magnetotelluric soundings, *Publ. Inst. Geophys. Pol. Acad. Sc.,* C-73(318), 63–81.

Nowozynski, K. & Pushkarev, P.Yu., 2001. The efficiency analysis of programs for two-dimensional inversion of magnetotelluric data, *Phys. Solid Earth,* **37**(6), 503–516.

Pharaoh, T.C., 1999. Paleozoic terranes and their lithospheric boundaries within the Trans-European Suture Zone (TESZ): a review, *Tectonophysics,* **314,** 17–41.

Plewa, M., Plewa, S., Sroka, K. & Smiszek, R., 1995. New determinations of the terrestrial heat flow in Poland, *Bull. Pol. Acad. Sci., Earth Sci.,* **43**(4), 207–223.

Rokityanskiy, I.I., Amirov, V.K., Kulik, S.N. & Logvinov, I.M., 1975. The electrical conductivity anomaly in the Carpathians, *Acta Geod. Geophys. Mont.,* **10,** 277–286.

Schmucker, U. & Jankowski, J., 1971. Geomagnetic induction studies and the electrical state of the upper mantle, *Tectonophysics,* **13** (1–4), 233–256.

Semenov, V.Yu., 2000. On the apparent resistivity in magnetotelluric sounding, *Phys. Solid Earth,* **36**(1), 99–100.

Semenov, V.Yu. & Jozwiak, W., 2005. Estimation of the upper mantle electric conductance at the Polish margin of the East-European Platform, *Phys. Solid Earth,* **41**(4), 326–322.

Semenov, V.Yu. & Kaikkonen, P., 1986. On magnetotelluric data analysis with example for the Kuhmo region in eastern Finland, *Geophys. Dept. Oulu Univ., Finland, Report,* **13,** 1–13.

Semenov, V.Yu., Jankowski, J., Ernst, T., Jozwiak, W., Pawliszyn, J. & Lewandowski, M., 1998. Electromagnetic soundings across the Holy Cross Mountains, *Acta Geophys. Pol.,* **46**(2), 171–187.

Semenov, V.Yu., Jankowski, J. & Jozwiak, W., 2002. New evidence of the anomalously conductive mantle beneath the Tornquist-Teisseyre zone in Poland, *Acta Geophys. Pol.,* **50**(4), 517–526.

Semenov, V.Yu., Jozwiak, W. & Pek, J., 2003. Deep electromagnetic soundings conducted in Trans-European Suture Zone, *EOS Transactions,* **84**(52), 581–584.

Siripunvaraporn, W. & Egbert, G., 2000. An efficient data-subspace inversion method for 2D magnetotelluric data, *Geophysics,* **65,** 791–803.

Smirnov, M. & Pedersen, L.B., 2005. Geoelectrical structure of Sorgenfrei-Tornquist Zone in southern Sweden and Denmark. EGU General Assembly, Vienna, Austria, April 2005.

Sroda, S. *et al.*, and CELEBRATION 2000 Working Group, 2006. Crustal and upper mantle structure of the Western Carpathians from CELEBRATION 2000 profiles CEL01 and CEL04: seismic models and geological implications. *Geophys. J. Int.*, **167**(2), 737–760.

Swift, C.M., 1967. Magnetotelluric investigation of an electrical conductivity anomaly in the south-western United States. *Dissertation*, MIT, Cambridge.

Varentsov, I. & EMTESZ-Pomerania WG, 2004. EMTESZ-Pomerania: an integrated EM sounding of the lithosphere in the Trans-European Suture Zone (NW Poland and NE Germany). Abstracts of the 17th Workshop on the Electromagnetic induction in the Earth (India, Hyderabad).

Wieladek, R. & Ernst, T., 1977. Application of the method of least squares to determining impulse responses and transfer functions. *Publ. Inst. Geophys. Pol, Acad. Sc.,* **G-1** (110), 3–12.

Wieladek, R., Nowozynski, K., Tarlowski, Z., 1981. Application of the Cholesky-Banachiewich method to solving some linear systems of equations approximating Helmholtz's equation. *Publ. Inst. Geophys. Pol. Acad. Sc.,* **G-2** (12), 3–12.

Wybraniec, S., 1999. Transformations and visualization of potential field data, *Polish Geol. Inst., Special Papers,* **1,** 1–88.

Zielhuis, A. & Nolet, G., 1994. Deep seismic expression of an ancient plate boundary in Europe, *Science,* **265,** 79–81.

Znosko, J., 1998. Atlas tektoniczny Polski (Tectonic atlas of Poland). Panstw. Inst. Geol. i Wydawn. Kartogr., Warszawa.